CONTRAST MEDIA &
MOLECULAR IMAGING

Full Paper

First *in vivo* MRI assessment of a self-assembled metallostar compound endowed with a remarkable high field relaxivity

J.B. Livramento[1], C. Weidensteiner[2], M.I.M. Prata[3], P.R. Allegrini[2], C.F.G.C. Geraldes[4], L. Helm[1], R. Kneuer[2], A.E. Merbach[1]*, A.C. Santos[3], P. Schmidt[2] and É. Tóth[1,5]

[1]*Laboratoire de Chimie Inorganique et Bioinorganique, Ecole Polytechnique Fédérale de Lausanne, EPFL-BCH; CH-1015 Lausanne, Switzerland*
[2]*Novartis Institutes for BioMedical Research, Basel, Switzerland*
[3]*Instituto de Biofísica e Biomatemática, Faculdade de Medecina, Universidade de Coimbra, Coimbra, Portugal*
[4]*Departamento de Bioquímica, Centro de RMN e Centro de Neurociências e Biologia Celular, Faculdade de Ciências e Tecnologia, Universidade de Coimbra, Coimbra, Portugal*
[5]*Centre de Biophysique Moléculaire, CNRS, rue Charles-Sadron, 45071 Orléans, Cedex 2, France*

ABSTRACT: $\{Fe[Gd_2bpy(DTTA)_2(H_2O)_4]_3\}^{4-}$ is a self-assembled, metallostar-structured potential MRI contrast agent, with six efficiently relaxing Gd^{3+} centres confined into a small molecular space. Its proton relaxivity is particularly remarkable at very high magnetic fields ($r_1 = 15.8\,\mathrm{mM^{-1}\,s^{-1}}$ at 200 MHz, 37°C, in H_2O). Here we report the first *in vivo* MRI feasibility study, complemented with dynamic γ scintigraphic imaging and biodistribution experiments using the ^{153}Sm-enriched compound. Comparative MRI studies have been performed at 4.7 T in mice with the metallostar and the small molecular weight contrast agent gadolinium(III)-1,4,7,10-tetraazacyclododecane-1,4,7,10-tetraacetate ($[Gd(DOTA)(H_2O)]^- = GdDOTA$). The metallostar was well tolerated by the animals at the concentrations of 0.0500 (high dose) and 0.0125 (low dose) mmol Gd kg^{-1} body weight; (BW). The signal enhancement in the inversion recovery fast low angle shot (IR FLASH) images after the high-dose metallostar injection was considerably higher than after GdDOTA injection (0.1 mmol Gd kg^{-1} BW), despite the higher dose of the latter. The high-dose metallostar injection resulted in a greater drop in the spin-lattice relaxation time (T_1), as calculated from the inversion recovery true fast imaging with steady-state precession (IR TrueFISP) data for various tissues, than the GdDOTA or the low dose metallostar injection. In summary, these studies have confirmed that the approximately four times higher relaxivity measured *in vitro* for the metallostar is retained under *in vivo* conditions. The pharmacokinetics of the metallostar was found to be similar to that of GdDOTA, involving fast renal clearance, a leakage to the extracellular space in the muscle tissue and no leakage to the brain. As expected on the basis of its moderate molecular weight, the metallostar does not function as a blood pool agent. The dynamic γ scintigraphic studies performed in Wistar rats with the metallostar compound having ^{153}Sm enrichment also proved the renal elimination pathway. The biodistribution experiments are in full accordance with the MR and scintigraphic imaging. At 15 min post-injection the activity is primarily localized in the urine, while at 24 h post-injection almost all radioactivity is cleared from tissues and organs. Copyright © 2006 John Wiley & Sons, Ltd.

KEYWORDS: magnetic resonance imaging; contrast agents; gadolinium; *in vivo*; pharmacokinetics; biodistribution; γ imaging

Correspondence to: A. E. Merbach, Laboratoire de Chimie Inorganique et Bioinorganique, Ecole Polytechnique Fédérale de Lausanne, EPFL-BCH 3110, CH-1015 Lausanne, Switzerland.
E-mail: andre.merbach@epf1.ch

Abbreviations used: bpm, beats per minute; BW, body weight; CA, contrast agent; $C(t)$, gadolinium concentration time course in tissue or blood; DCE, dynamic contrast enhanced; FLASH, fast low angle shot, fast gradient echo MRI method; FOV, field of view; C_{Gd}, gadolinium concentration; GdDOTA, gadoterate meglumine, type of MR contrast agent; HSA, human serum albumin; IR, inversion recovery; RARE, rapid acquisition and relaxation enhancement, fast spin echo MRI method; T_1, spin-lattice relaxation time in MR; TE, echo time; TI, inversion time; TR, repetition time; TrueFISP, inversion recovery true fast imaging with steady state precession, fast steady state free precession MRI method.

INTRODUCTION

Over the last two decades, magnetic resonance imaging (MRI) has grown into one of the most prominent modalities in medical diagnostics. This primarily non-invasive technique allows high-resolution images of a given part of the body to be obtained. The successful history of MRI, which was awarded the 2003 Nobel Prize for Physiology and Medicine, has been largely assisted by the concomitant development of MRI contrast agents (CA) (1). These drugs—Gd^{III} complexes in the majority—enhance the image contrast by accelerating the water proton relaxation in the surrounding tissues. The efficacy

WILEY InterScience®
DISCOVER SOMETHING GREAT

of a contrast agent is commonly measured by its millimolar relaxivity (r_1), which is the ability of the paramagnetic agent to enhance the longitudinal proton relaxation rate, referred to 1 mM concentration (of Gd^{III}). The currently marketed MRI contrast agents display relaxivities around 4–5 $mM^{-1} s^{-1}$; however the Solomon–Bloembergen–Morgan theory predicts much higher values for Gd^{III} complexes, provided the rotation and electron spin relaxation are slow and the water exchange rate between the inner sphere and the bulk solvent is optimal (2).

Several emerging MRI applications, first of all in the field of molecular imaging, require very high efficacy contrast agents (3). It implies both high molar relaxivity per Gd^{III} and high relaxivity concentrated into a limited molecular volume. In the perspective of developing contrast agents that concentrate high relaxivity into a small molecular space, we have recently started exploiting heterometallic assemblies. We have reported the synthesis (4) and physicochemical characterization (5) of a heterotritopic, bipyridine derivative poly(amino carboxylate) ligand which is capable of self-assembling with Gd^{III} and Fe^{II} into a rigid metallostar structure $\{Fe[Gd_2bpy(DTTA)_2(H_2O)_4]_3\}^{4-}$ (Fig. 1). This compound possesses a high proton relaxivity, comparable to that of high generation dendrimers. Several key features contribute to the high relaxivity of the metallostar (5): (i) the rigidity of the metallostar originating from the non-flexible $Fe(bpy)_3$ core; (ii) the presence of six efficiently relaxing Gd^{III} metals within one molecule, each bearing two inner sphere water molecules (all commercially available contrast agents have a single inner sphere water); and (iii) the water exchange rate of the 12 water molecules is close to the optimal value. Moreover, with six Gd^{III} ions in a relatively low molecular mass of 3744 $g\,mol^{-1}$, the metallostar is a highly powerful contrast agent in terms of efficacy by unity mass. Indeed,

this compound represents the most concentrated paramagnetic relaxation effect among all Gd^{III}-based potential contrast agents ever reported (4).

Given the greater spatial resolution and sensitivity associated with higher frequencies, the current tendency in MRI is to increase the magnetic field. In the clinics today, most MRI machines work at 1.5–3 T. However, for experimental animal studies, much higher fields are commonly applied (up to 9.4 T or even higher) (3,6). Macromolecular contrast agents often have a high proton relaxivity peak centred between 20 and 60 MHz; however, above this frequency the longitudinal relaxivity strongly decreases with increasing field and, at high fields, macromolecular agents are hardly superior to small molecular weight chelates. The Solomon–Bloembergen–Morgan theory predicts that at frequencies above ~200 MHz the relaxivity increases with the inverse of the rotational correlation time τ_R, in contrast to lower frequencies, where it is proportional to τ_R. Consequently, at very high fields intermediate size molecules, such as the metallostar, are favourable over very large ones. Indeed, the metallostar has an unusually broad high field relaxivity peak centred at a relatively high frequency, and exceptionally high relaxivities above 60 MHz (Table 1). This high relaxivity, which is additionally confined to a small molecular space (high density of relaxivity), makes the metallostar a prime candidate for high-field MRI contrast agent applications.

Here we report the first *in vivo* MRI feasibility study with the metallostar as a potential medical MRI contrast agent. The pharmacokinetics and *in vivo* relaxivity were determined in mice and compared with those of a typical commercial, small molecular weight contrast agent, GdDOTA. In addition, to complement the MRI results we have performed dynamic γ scintigraphic and biodistribution studies in Wistar rats at short (10–15 min) and long (24 h) periods of time by using the
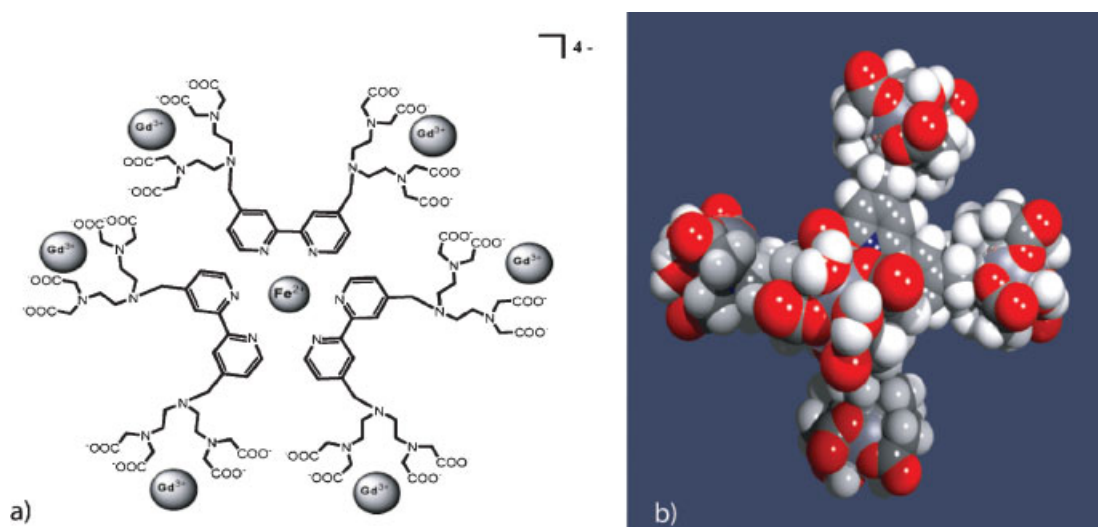
Figure 1. (a) Schematic structure and (b) molecular modeling representation of the metallostar $\{Fe[Gd_2bpy(DTTA)_2(H_2O)_4]_3\}^{4-}$.

Table 1. High-field proton molar relaxivities, r_1 (mM^{-1} s^{-1}), for GdDOTA and the metallostar measured in water

	200 MHz (4.7 T)		400 MHz (9.4 T)	
	25°C	37°C	25°C	37 °C
Metallostar	16.4	15.8	9.3	8.5
GdDOTA	4.0	3.0	3.9	3.0

^{153}Sm analogue metallostar compound, $\{Fe[^{153}Sm_2bpy(DTTA)_2(H_2O)_4]_3\}^{4-}$.

EXPERIMENTAL

The synthesis of the ligand $H_8bpy(DTTA)_2$ has been described in a previous communication (4). 153-Samarium chloride ($^{153}SmCl_3$) was produced at the ITN (Instituto Tecnológico e Nuclear), Lisbon, with a specific activity >5 GBq mg^{-1}. For this purpose a $^{153}Sm_2O_3$ was prepared from a 98% samarium-152 enriched samarium oxide target, sealed into a quartz vial and welded into an aluminium can, by neutron irradiation using a thermal flux of 2.3×10^{13} n cm^{-2} s^{-1}. Following irradiation, the sample was opened, dissolved in HCl (1 M) and the final $^{153}SmCl_3$ was brought to a stock concentration of 1.9 mM.

Sample preparation

A GdCl$_3$ solution was prepared from Gd$_2$O$_3$ of 99.9% purity (Fluka) by dissolution in excess HCl, which was evaporated off. The concentration of the metal ion was determined by complexometric titration with standardized Na$_2$H$_2$EDTA solution. $[Gd_2bpy(DTTA)_2(H_2O)_4]^{2-}$ was prepared by adding solid ligand to a solution of GdCl$_3$ in 1:2 molar ratio. The pH, measured with a calibrated combined glass electrode, was adjusted to 7.1 by addition of known amounts of NaOH (0.1 M). A slight ligand excess was used (3%) and the absence of free metal was checked by the xylenol orange test.

$\{Fe[Gd_2bpy(DTTA)_2(H_2O)_4]_3\}^{4-}$ was prepared by mixing a solution of $[Gd_2bpy(DTTA)_2(H_2O)_4]^{2-}$ with a freshly prepared solution of Fe^{II} ions [Fe(NH$_4$)$_2$(SO$_4$)·6H$_2$O] in 3:1 molar ratio. A slight excess of $[Gd_2bpy(DTTA)_2(H_2O)_4]^{2-}$ (3%) was used to insure complete Fe^{II} coordination. pH was set to 7.4 by addition of HCl (0.1 M). NaCl (0.9%) was added to avoid osmotic pressure problems upon injection. The final concentration of the Gd-metallostar solution was $C_{Gd} = 10.0$ mM.

$[Sm_2bpy(DTTA)_2(H_2O)_4]^{2-}$ was prepared by adding an excess of solid ligand to a solution of SmCl$_3$ (the concentration of the metal ion was determined by complexometric titration with standardized Na$_2$H$_2$EDTA solution). A solution of $^{153}SmCl_3$ was then added to the previous solution. The final solution contained a 3% excess ligand in respect to the overall samarium concentration to ensure complete metal coordination. pH was adjusted to 7.0 by addition of known amounts of NaOH (0.1 M).

$\{Fe[Sm_2bpy(DTTA)_2(H_2O)_4]_3\}^{4-}$ was prepared by mixing a solution of $[Sm_2bpy(DTTA)_2(H_2O)_4]^{2-}$ with a freshly prepared solution of Fe^{II} ions [Fe(NH$_4$)$_2$ (SO$_4$)·6H$_2$O] in 3:1 molar ratio. A slight excess of $[Gd_2bpy(DTTA)_2(H_2O)_4]^{2-}$ (3%) was used to ensure complete Fe^{II} coordination. pH was set to 7.4 by addition of known amounts of NaOH and HCl (both 0.1 M). The final concentration of the Sm-metallostar solution was $C_{Sm} = 18.9$ mM.

MRI

MR measurements were performed on a 4.7 T Bruker Biospec MR system (Bruker Biospin, Ettlingen, Germany) equipped with a 12 cm bore gradient system using a birdcage resonator with inner diameter of 35 mm.

For anatomical reference, a multislice rapid acquisition and relaxation enhancement (RARE) sequence was performed with the following parameters: RARE factor = 16, echo time (TE) = 10 ms, repetition time (TR) = 2.5 s, 15 axial slices (eight coronal slices), slice thickness 1.5 mm, field of view (FOV) = 3.3 cm × 3.3 cm (FOV = 4.5 cm × 4.5 cm), matrix = 256 × 128.

Regional contrast agent uptake was assessed with DCE-MRI with two different imaging methods:

(1) A series of IR FLASH images (7) was acquired using the following parameters: flip angle $\alpha = 12°$, $TE = 3.0$ ms, $TR = 6.9$ ms, 1 slice, slice thickness = 1.5 mm, matrix = 128 × 96, inversion delay 0.9 s, 256 repetitions with temporal resolution 6 s, duration 25 min. The imaging slice was either axial with FOV = 4.1 cm × 4.1 cm, or coronal oblique with FOV = 4.5 cm × 4.5 cm. CA was injected at repetition 8 (see below). Before the start of the DCE-MR image series, a reference image was acquired with the same sequence parameters but without the inversion pulse.

(2) A series of IR TrueFISP images (8) was acquired using following parameters: flip angle $\alpha = 30°$, $TE = 1.69$ ms, $TR = 3.38$ ms, range of inversion time (TI) = 210–2480 ms, 1 axial slice, slice thickness = 2.0 mm, FOV 30 mm × 22.5 mm. Matrix was 64 × 48, TI increment (i.e. acquisition time for one frame) was 162 ms, number of frames was 16. The IR TrueFISP block was repeated 80 times. The temporal resolution (i.e. time period between the start of two successive image blocks) was 10 s before CA injection at repetition 8, and 8 s thereafter. The overall experimental duration was 12 min.

Metallostar:
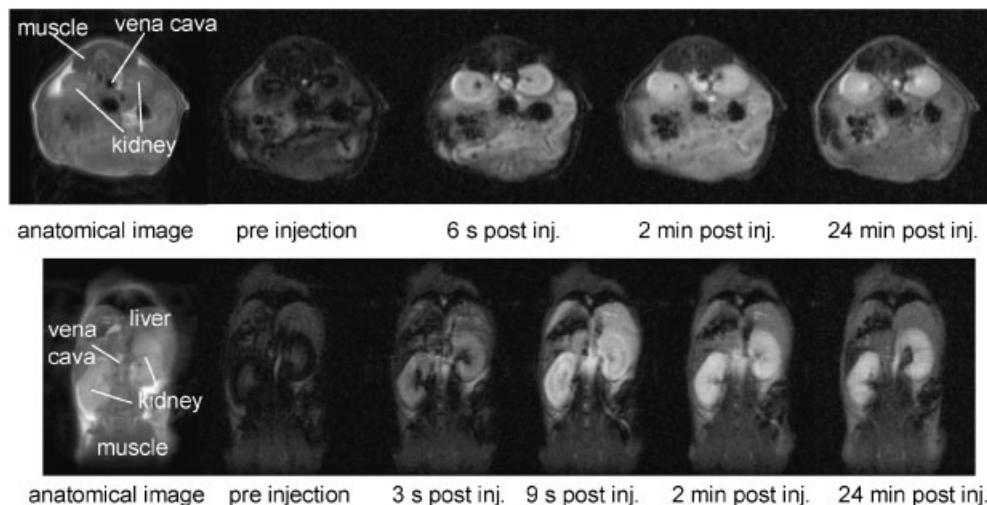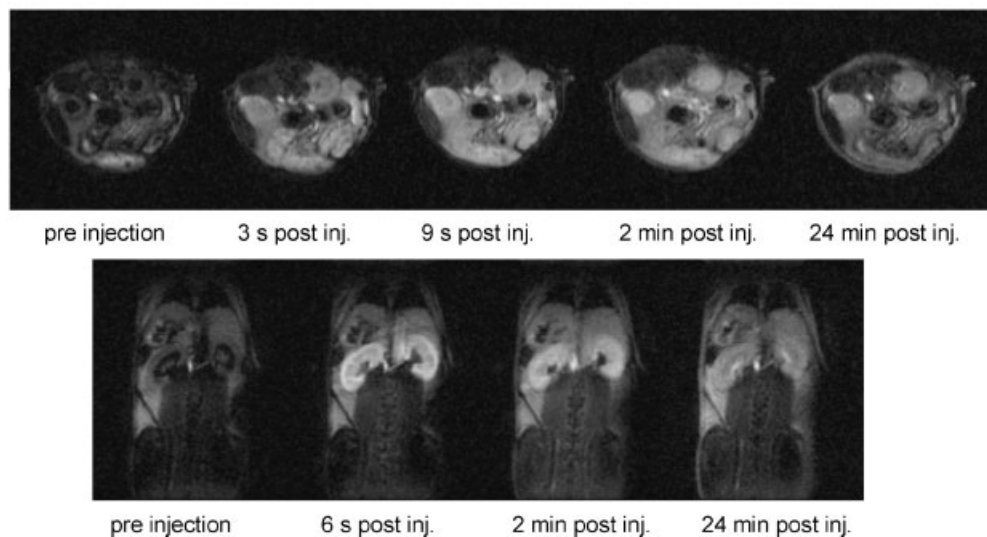
Figure 2. IR FLASH images taken at different times of the DCE-MRI experiment in mice. Rows 1 and 2 represent the high-dose metallostar (0.05 mmol Gd kg^{-1} BW) injection, whereas rows 3 and 4 represent the GdDOTA (0.1 mmol Gd kg^{-1} BW) injection. Rows 1 and 3 show axial slices, and rows 2 and 4 coronal slices. The first images of rows 1 and 2 are anatomical RARE images.

All MRI studies were performed in strict adherence to the Swiss law for animal protection. *In vivo* experiments were performed in female C57/BL6 mice ($n = 8$, 20–25 g, obtained from Charles River Laboratories France). The group sizes were $n = 3$ for the IR FLASH experiments and $n = 5$ mice for the IR TrueFISP experiments. The mice were anaesthetized with isoflurane (1.5–2.5%) in an O_2–N_2O 1:2 mixture applied with a face mask allowing free breathing. The temperature was kept at 38°C with a current of warm air, and the respiration was monitored (using a balloon taped to the abdomen and connected to a pressure transducer). In three animals respiration rate, heart rate (with electrocardiogram electrodes attached to the front paws), and body temperature (with an intrarectal temperature probe) were recorded during the experiment with GdDOTA and metallostar injection with two different doses, respectively. The metallostar was injected as a bolus via a tail vein catheter with an infusion pump (3 ml min^{-1}) at a dose of 0.05 mmol Gd kg^{-1} body weight (BW) (high dose) or 0.0125 mmol Gd kg^{-1} BW (low dose), i.e. 5 or 1.25 µl g^{-1} 1 BW of the CA solution were injected. For comparison, the experiments were repeated in the same mice with injection of the clinically approved small molecular weight CA GdDOTA (Dotarem, Guerbet, France). A dose of

$0.1\,\mathrm{mmol\,Gd\,kg^{-1}}$ BW was injected via a tail vein catheter, corresponding to $0.2\,\mu\mathrm{l\,g^{-1}}$ BW CA solution.

MRI data processing

CA concentration was calculated from the change in signal intensity $S(t)$ in the DCE-MRI series with software tools developed in-house with the IDL 6.1 programming environment (Research Systems Inc., Boulder, CO, USA). T_1 maps were calculated for each time point on a pixel-by-pixel basis from each image using the standard IR equation (9) for the IR FLASH images,

$$T_1 = \frac{-TI}{\ln\left(0.5\left(1 - \frac{S}{S_0}\right)\right)} \qquad (1)$$

where TI is the inversion time and S_0 is the signal intensity in the pre-contrast reference image.

For the IR TrueFISP images, a three-parameter fit of the signal time course $S(t)$ over the eight image frames (with different inversion delays t) was performed using the following model function (10):

$$S(t) = S_{stst}\left[1 - INV \cdot \mathrm{e}^{-(t/T_1^*)}\right] \qquad (2)$$

where T_1^* is the apparent relaxation time, S_{stst} the steady state signal, and INV the inversion factor (i.e. the ratio between the absolute signals at $TI = 0$ and S_{stst}). T_1^* was computed using a least-square fitting routine.

T_1 was calculated for each time point from the following equation (10):

$$T_1 = T_1^* \cos\frac{\alpha}{2}(INV - 1) \qquad (3)$$

where α is the excitation flip angle.

Apparent Gd concentrations, C_{Gd}, were then calculated (for both IR FLASH and IR TrueFISP experiments) for each time point with the following formula:

$$C_{\mathrm{Gd}} = \frac{(1/T_1) - (1/T_{10})}{r_1} \qquad (4)$$

using the molar relaxivities r_1 of $13.5\,\mathrm{s^{-1}\,mM^{-1}}$ per Gd for the metallostar (measured in saline at 4.7 T and 37°C) and $3.3\,\mathrm{s^{-1}\,mM^{-1}}$ for GdDOTA [measured in water with 4% human serum albumin (HSA) at 4.7 T and 37°C; personal communication, Guerbet]. T_{10} was the mean baseline T_1, i.e. the mean of the first seven scans.

Mean gadolinium concentration time courses $C(t)$ were calculated in several regions of interests (ROIs): skeletal muscle, kidney cortex and medulla, brain, liver and blood pool in the jugular vein.

Biodistribution and γ imaging

A γ camera-computer system (GE 400 GenieAcq, from General Electric, Milwaukee, USA) was used for acquisition and pre-processing. Data processing and display were performed on a personal computer using a homemade software developed for the IDL 5.2 computer tool. A well counter (DPC-Gamma C_{12}, LA, USA) with a Compaq DeskPro compatible computer was used for activity counting in the biodistribution studies.

γ–Images were obtained and biological distribution of the ^{153}Sm-metallostar complex was determined using 200 g Wistar rats (used as groups of four; provided by Charles River Laboratory Barcelona, Spain). All animal studies were carried out in compliance with procedures approved by the appropriate institutional review committees. Conscious rats were allowed free access of food and water *ad libitum*. Four animals were anaesthetized with ketamine $(50\,\mathrm{mg\,ml^{-1}})$–chloropromazine (2.5%) (10:3) and injected in the femoral vein with ca. $200\,\mu\mathrm{Ci}$ of ^{153}Sm-metallostar. The animals were then positioned in ventral *decubitus* over the detector. Image acquisition was initiated immediately before radiotracer injection. Sequences of 120 images (of 5 s each) were acquired to 64×64 matrices. Images were subsequently processed using an IDL-based program. In order to analyze the transport of radiotracer over time, four ROI were drawn on the image files, corresponding to the thorax, liver, left kidney and bladder. The time–activity curves were obtained from these regions. Animals were sacrificed 15 min after injection and the major organs removed were weighed and counted in a γ well-counter. Similar biodistribution studies with a group of four rats sacrificed 24 h after i.v. injection of ^{153}Sm-metallostar were also performed.

RESULTS AND DISCUSSION

Magnetic resonance imaging

Effect of the metallostar on vital functions. The CA was well tolerated by the mice. No gross side effects were observed during injection, immediately or days after the experiment. In the high-dose metallostar experiments $(0.05\,\mathrm{mmol\,Gd\,kg^{-1}}$ BW), a drop in the respiration frequency of approximately 25% (from 28 to 19 bpm) and a drop in the heart rate of approximately 10% (from 450 to 405 bpm) were observed in the first minute post-injection. Five minutes post injection, the values returned to the pre-injection level. No such drop was observed after GdDOTA or the lower dose metallostar injection. After all three types of injection, the body temperature slightly increased (approximately 0.2°C). Overall, the metallostar seemed to be harmless to the animals; however, a more in-depth study should be performed to further assess its toxicology.

DCE-MRI *in vivo*. Comparison between the metallostar and GdDOTA. IR FLASH images of the dynamic contrast enhanced MRI (DCE-MRI)
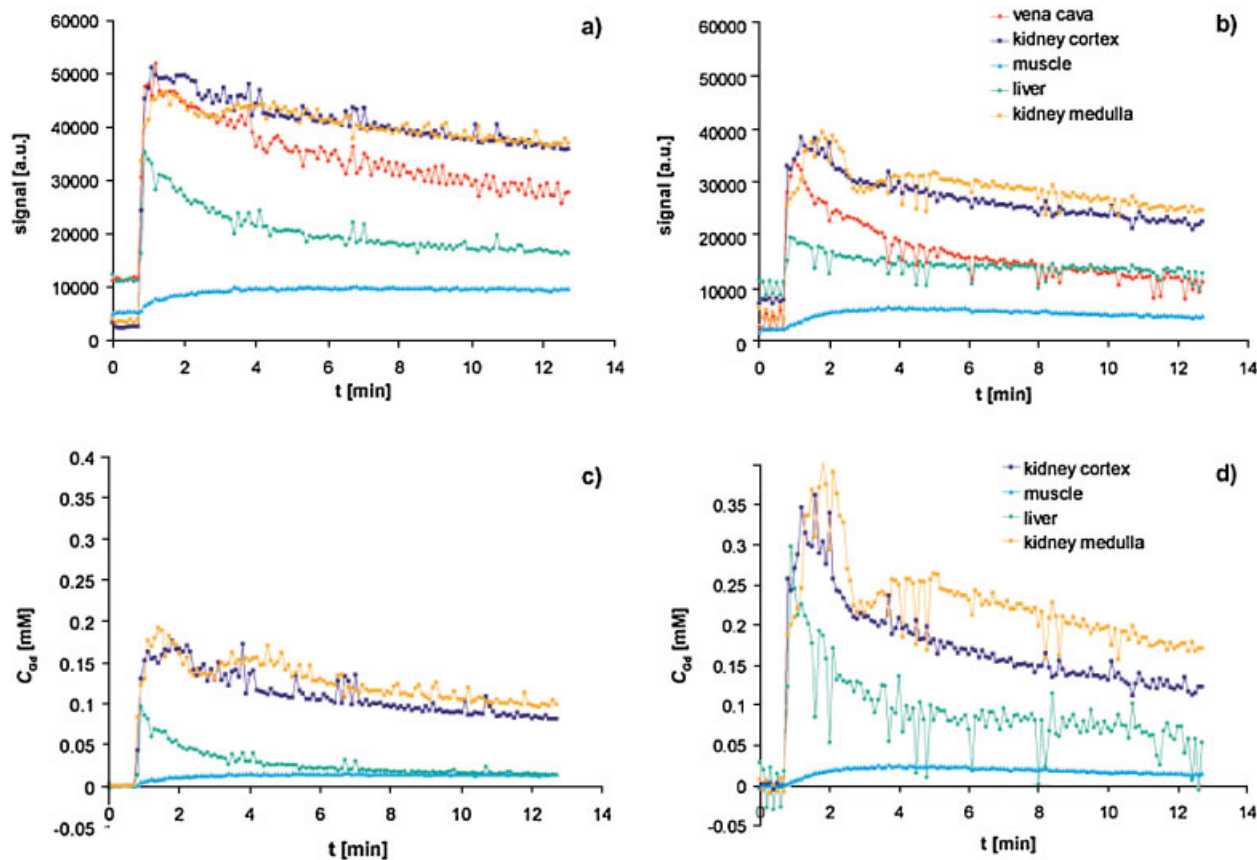
experiment with the metallostar (high dose; 0.05 mmol-Gd kg^{-1} BW) and GdDOTA (0.1 mmol Gd kg^{-1} BW) are displayed in Fig. 2. In the pre-injection image, the vena cava, kidneys and muscle were dark due to the particular inversion delay chosen. After injection, the kidneys and vena cava were lit up as a result of T_1 shortening. A slight enhancement in the paravertebral muscle and liver was also observed for both CAs.

The signal intensity time courses of the IR FLASH images are displayed in Fig. 3 (top). The scattering in the curves was caused by animal motion. Despite its lower dose, the metallostar resulted in a considerably higher signal enhancement as compared with GdDOTA (the same MRI method and acquisition parameters were used). This finding is in full accordance with the remarkably higher *in vivo* relaxivity of the metallostar compared to GdDOTA (see below).

The gadolinium concentration time courses, $C(t)$, were calculated from the IR FLASH data and are shown in Fig. 3 (bottom). In the different tissues, the Gd concentration was found to be approximately twice as high for GdDOTA than for the metallostar (high dose). This is in accordance with the double injected dose of GdDOTA as compared with the metallostar. For both CAs, an enrichment of Gd was observed after 4–5 min in the kidney medulla.

The T_1 time courses calculated from the IR TrueFISP data are shown in Fig. 4. Baseline T_1 values (before injection) varied slightly between individuals. The T_1 drop after the high-dose metallostar injection (0.05 mmol Gd kg^{-1} BW) was larger than the drop after GdDOTA injection and also, as expected, larger than for the low-dose metallostar (0.0125 mmol Gd kg^{-1} BW). These results confirm again the higher relaxivity of the metallostar. $C(t)$ curves calculated from these data are also displayed in Fig. 4. In several types of tissues, the Gd concentration was 2–4 times lower for the low dose (0.0125 mmol Gd kg^{-1} BW) as compared with the high dose (0.05 mmol Gd kg^{-1} BW) of the metallostar. Theoretically a factor of 4 was to be expected for all tissue types. Comparing the high-dose metallostar and the GdDOTA data, a factor of approximately 2 between the Gd concentrations was found in brain and muscle, while the ratio was smaller in the kidney cortex.

Pharmacokinetics. The time course of biodistribution, based on the observation of the CA uptake in the different ROIs, was found to be similar for the metallostar and GdDOTA (Fig. 3). Both CAs are primarily eliminated by the kidneys from the blood stream, as indicated by the high Gd accumulation in the kidney medulla. The data

Figure 3. Top row: time course of signal intensity (up to 12 min post injection) in several regions of interest during IR FLASH DCE-MRI experiments in mice with the (a) metallostar (dose 0.05 mmol Gd kg^{-1} BW) and (b) GdDOTA (dose 0.1 mmol Gd kg^{-1} BW). Bottom row: time course of Gd concentration (up to 12 min post-injection) calculated from the DCE-MRI data for (c) metallostar and (d) GdDOTA. The time courses are data from individual animals.
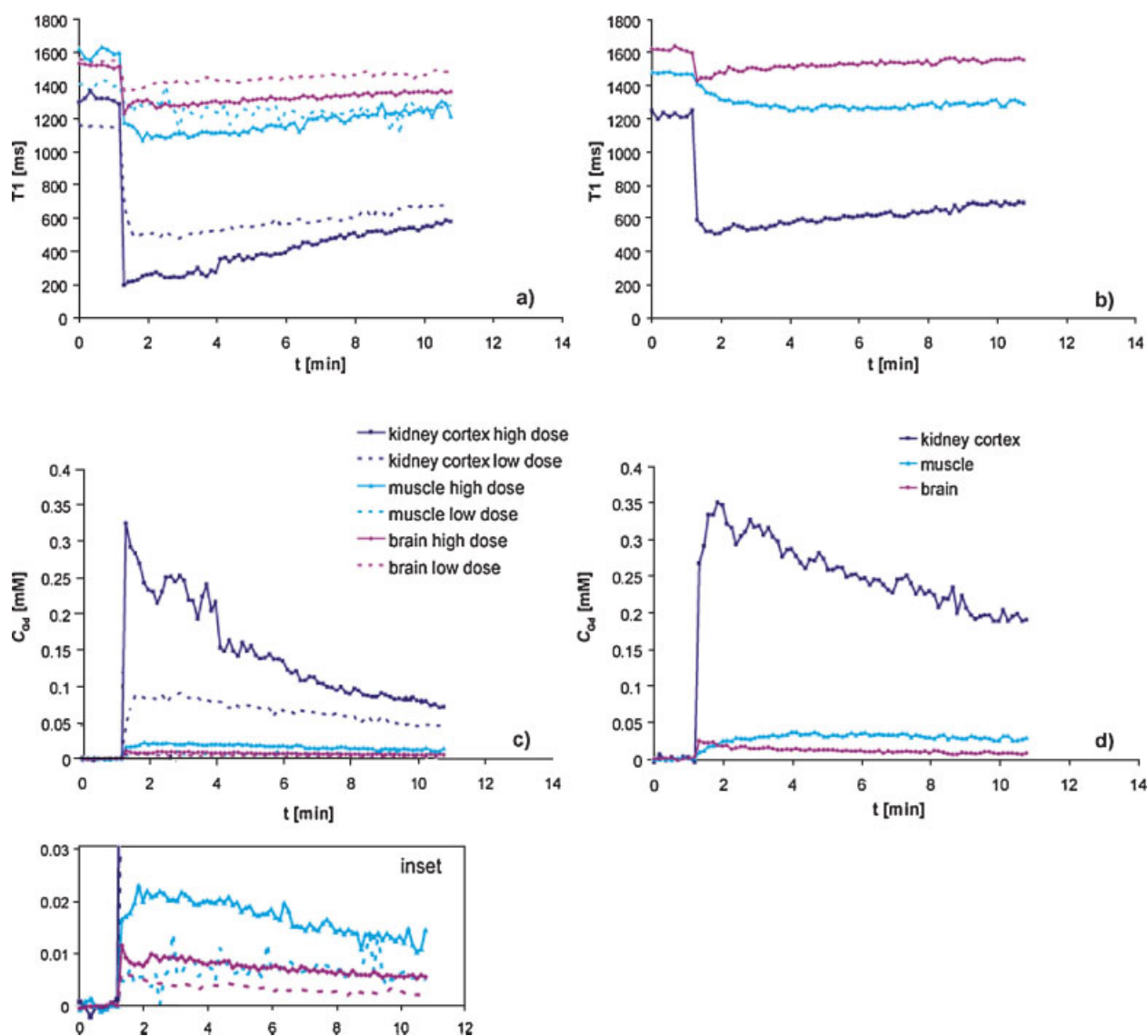
Figure 4. Top row: time course of T_1 (up to 10 min post-injection) in several regions of interest during IR TrueFISP DCE-MRI experiments with the (a) metallostar and (b) GdDOTA in mice. Bottom row: time course of Gd concentration calculated from the previous data for the (c) metallostar (with enlarged insert) and (d) GdDOTA. High (low) dose of metallostar was 0.05 (0.0125) mmol Gd kg^{-1} BW. Dose of GdDOTA was 0.1 mmol Gd kg^{-1} BW. The time courses are data from individual animals.

obtained here are in accordance with previous reports on the pharmacokinetics of GdDOTA (11) or other small molecular weight Gd-based contrast agents (12).

For both CAs, the signal and concentration curves in the liver revealed a steady decrease to a low plateau value after the initial steep rise. This points to a small retention of both CA in the liver, as expected given their relatively small molecular weight.

Both CAs present limited T_1 changes and derived Gd concentration in the brain, as compared with kidney and liver (Fig. 4). This reflects the lower blood volume in the brain compared with kidney and liver and the action of the blood–brain barrier. The shape of the curve—a steep rise immediately after CA injection and slow decay thereafter—indicates that there is no leakage to the brain

parenchyma due to the intact blood—brain barrier. A different time course was observed in the muscle: the maximum was reached 2–3 min after injection. This can be rationalized in terms of a leakage of the CA to the extracellular space in the muscle tissue. The Gd concentration time courses in muscle indicated that, similarly to GdDOTA, the metallostar is not a blood pool agent due to the relatively small size of the molecule.

Gd concentration in the blood pool could not be calculated correctly with the IR FLASH method. Immediately after CA injection, very high CA concentrations occur in the blood vessels and in the kidney. At such high local concentrations T_2 is shortened by the CA, leading to a signal reduction. This effect was not corrected in the IR FLASH method, which yielded too
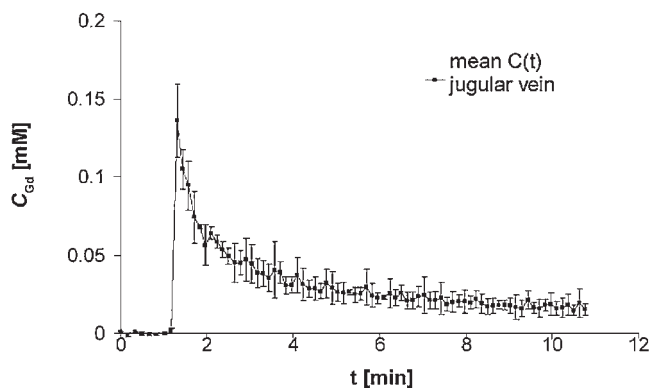
Figure 5. Time course $C(t)$ of mean blood Gd concentration (up to 10 min post-injection) measured in the jugular vein ($n = 3$, mean $\pm$ SD) calculated from IR TrueFISP DCE-MRI data with the metallostar (0.0125 mmol Gd kg^{-1} BW).

low T_1 values and thus Gd concentration in blood and—in some cases—also in the kidney. Therefore, the experiments were also performed with the IR TrueFISP method which is in this respect superior to the IR FLASH method: (1) T_2 effects are taken into account because the method also yields T_2; (2) it has a higher accuracy for T_1 determination than the IR FLASH method since 16 inversion delays are included instead of just one.

The time course $C(t)$ of the mean blood Gd concentration could then be successfully assessed for the lower metallostar dose (0.0125 mmol Gd kg^{-1} BW) in the jugular veins in the neck. The average of three veins in two animals is shown in Fig. 5. During the first 2 min post injection, the Gd concentration decreased rapidly, followed by a slower decay.
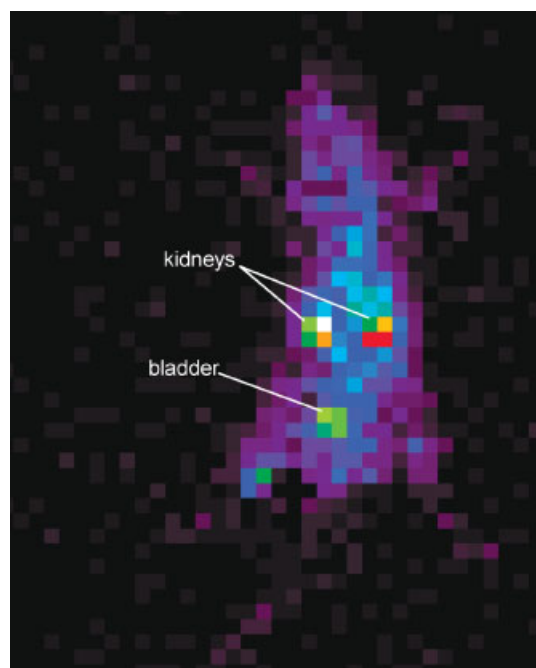
Figure 6. Scintigraphic dynamic image obtained 200 seconds after injection of ^{153}Sm-metallostar i.v. in a Wistar rat.

Based on the injected dose of 0.0125 mmol Gd kg^{-1} BW and a blood volume of 1.5 ml for a mouse with 20 g BW, the theoretical Gd concentration in blood is 0.17 mM. Initial (8 s post-injection) Gd concentration derived in the jugular veins for this metallostar dose was approximately 0.12 mM. The close agreement between the theoretical and experimental values reveals that the *in vivo* relaxivity of the metallostar is very close to the value of 13.5 s^{-1} mM^{-1} measured in saline.

## Biodistribution and dynamic scintigraphic studies

To complement the MRI data, biodistribution and dynamic γ scintigraphic studies were performed in Wistar rats using a metallostar solution where the gadolinium was replaced by a mixture of radioactive and non-radioactive samarium (13,14). The scintigraphic image obtained 200 s after tracer injection of ^{153}Sm-metallostar is shown in Fig. 6. The results are in agreement with the MRI observations, i.e. the main activity is found to be located in the kidneys and bladder, which is the excretion pathway for this small and hydrophilic complex. In addition, a very rapid clearance from all other organs is also proved. The time–activity curves for the ^{153}Sm-metallostar, obtained from the dynamic acquisition experiments, are shown in Fig. 7. The curves were smoothed and normalized in relation to the maximum activity obtained. Once again it is possible to observe that the metallostar undergoes an early clearance by the kidneys. The liver–spleen curve is similar to the thorax curve, corresponding only to blood activity. The fast blood elimination of the metallostar is indicative of its stability in terms of decomplexation and Gd release. Indeed, slower blood clearance is observed for less stable Gd^{III} complexes, due to reactions occurring in serum and leading to the dissociation of the chelate (11).

The characteristics of renal clearance and rapid washout of ^{153}Sm-metallostar were further investigated by biodistribution studies in Wistar rats. The results obtained at 15 min post-injection are summarized in Fig. 8. The highest activity was found to be present in the urine (% ID g^{-1} in urine 7.3 ± 4.2), which supports the MRI and scintigraphic results obtained. It is noteworthy that the urine had a red colour, characteristic of the Fe(bpy)$_3$ complex. It indicates that the Fe(bpy)$_3$ core of the metallostar structure remains intact even under *in vivo* conditions (although this was not quantified). Biodistribution was also carried out at 24 h (data not shown). These results show that almost all the radioactivity was cleared from tissues and organs. Only very slight deposition (less than 0.01 %) in the bone and liver/ spleen could be observed and may be related to a very small degree of samarium decomplexation (15,16).
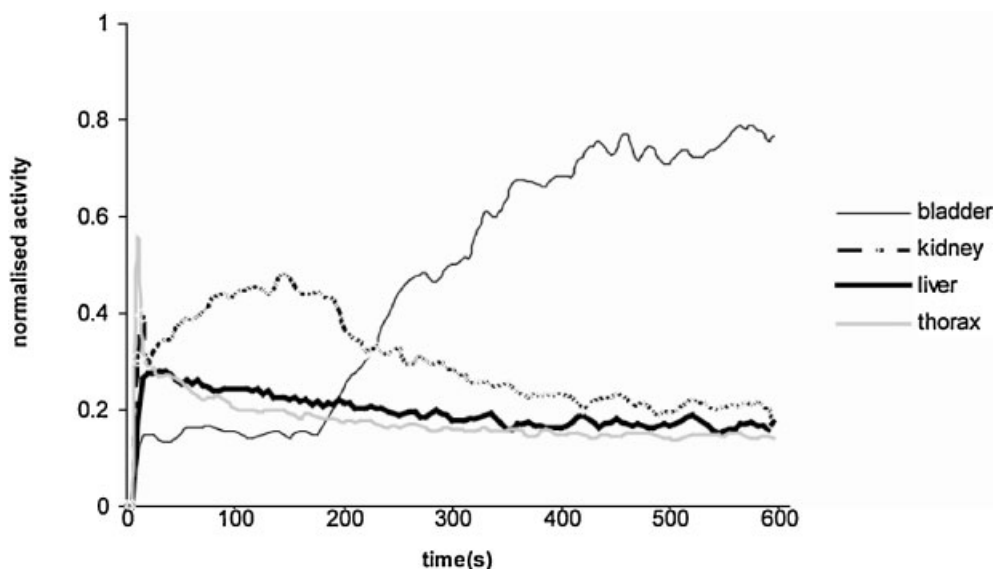
Figure 7. Time–activity curves obtained from dynamic images for the various regions of interest. The *y*-axis represents the normalized activity.
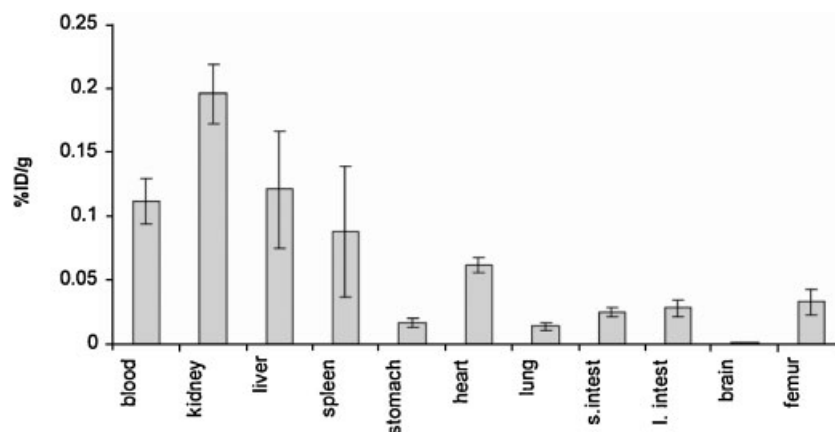
Figure 8. Biodistribution, stated as percentage of injected dose per gram of organ (%ID g^{-1} ±SD), of ^{153}Sm-metallostar in Wistar rats 15 min after i.v. injection. Results are the means of four animals.

The biodistribution shows as well that the metallostar does not cross the blood–brain barrier, as predicted by MRI and as expected for non-lipophilic complexes.

scintigraphic and MRI results. As expected, the activity is overwhelmingly localized in the urine that still presents the characteristic red color of the metallostar solution thus attesting the stability of the metallostar.

CONCLUSIONS

MRI studies conducted at 4.7 T in mice have confirmed that the metallostar displays approximately four times higher *in vivo* relaxivity than the commercially available GdDOTA. Furthermore, it was possible to determine that the metallostar has similar pharmacokinetics to that of GdDOTA, both contrast agents being eliminated from the blood stream by the kidneys in mice. Dynamic scintigraphic studies performed on a metallostar with ^{153}Sm enrichment confirm this elimination pathway in rats. Biodistribution experiments done in different periods of time (15 min and 24 h) proved to be in agreement with the

Acknowledgements

Tecnológico e Nuclear), Lisbon, for providing the $^{153}SmCl_3$.

REFERENCES

1. Caravan P, Ellison JJ, McMurry TJ, Lauffer RB. Gadolinium(III) Chelates as MRI contrast agents: structure, dynamics, and applications. *Chem. Rev.* 1999; **99**(9): 2293–2352.
2. Tóth E, Helm L, Merbach AE. Relaxivity of Gd(III) complexes: theory and mechanism. In *The Chemistry of Contrast Agents in Medical Magnetic Resonance Imaging*, Tóth E, Merbach AE (eds). Chichester: Wiley, 2001.
3. Pautler RG, Fraser SE. The year(s) of the contrast agent—micro-MRI in the new millennium. *Curr. Opin. Immunol.* 2003; **15**(4): 363–476.
4. Livramento JB, Tóth É, Sour A, Borel A, Merbach AE, Ruloff R. High relaxivity confined to a small molecular space: a metallostar-based, potential MRI contrast agent. *Angew. Chem. Int. Edn* 2005; **44**: 1480–1484.
5. Livramento JB, Sour A, Borel A, Merbach AE, Tóth É. Six Gd^{3+} ions densely packed within a starburst-shaped heterometallic compound. *Chem. Eur. J.* 2006; **12**: 989–1003.
6. Pautler RG. Mouse MRI: concepts and applications in physiology. *Physiology* 2004; **19**: 168–175.
7. Haase A, Matthaei D, Bartkowski R, Duhmke E, Leibfritz D. Inversion recovery snapshot FLASH MR imaging. *J. Comput. Assist. Tomogr.* 1989; **13**: 1036–1040.
8. Scheffler K, Hennig J. T_1 quantification with inversion recovery TrueFISP. *Magn. Reson. Med.* 2001; **45**: 720–723.
9. Jivan A, Horsfield MA, Moody AR, Cherryman GR. Dynamic T_1 measurement using snapshot-FLASH MRI. *J. Magn. Reson.* 1997; **127**: 65–72.
10. Schmitt P, Griswold MA, Jakob PM, Kotas M, Gulani V, Flentje M, Haase A. Inversion recovery TrueFISP: quantification of T_1, T_2, and spin density. *Magn. Reson. Med.* 2004; **51**: 661–667. [Erratum in Magn. Reson. Med. 2004; 52: 698].
11. Tweedle MF, Eaton SM, Eckelman WC, Gaughan GT, Hagan JJ, Wedeking PW, Yost FJ. Comparative chemical structure and pharmacokinetics of MRI contrast agents. *Invest. Radiol.* 1988; **23** (suppl. 1): S236–S239.
12. Harpur ES, Worah D, Hals PA, Holtz E, Furuhama K, Nomura H. Preclinical safety assessment and pharmacokinetics of gadodiamide injection, a new magnetic resonance imaging contrast agent. *Invest. Radiol.* 1993; **28** (suppl. 1): S28–S43.
13. Prata MIM, Santos AC, Neves M, Geraldes CFGC, Lima JJP. $^{153}Sm^{3+}$ and $^{111}In^{3+}$ DTPA derivatives with high hepatic specificity: *in vivo* and *in vitro* studies. *J. Inorg. Biochem.* 2002; **91**: 312–319.
14. Alves FC, Donato P, Sherry AD, Zaheer A, Zhang S, Lubag AJM, Merritt ME, Lenkinsky RE, Frangioni JV, Neves M, Prata MIM, Santos AC, Lima JJP, Geraldes CFGC. Silencing of phosphonate-gadolinium magnetic resonance imaging contrast by hydroxyapatite binding. *Invest. Radiol.* 2003; **38**(12): 750–760.
15. Vallabhajosula SR, Harwig JF, Siemsen JK, Wolf W. Radiogallium localization in tumors: blood binding and transport and the role of transferrin. *J. Nucl. Med.* 1980; **21**: 650–656.
16. Subramanian KM, Wolf W. A new radiochemical method to determine the stability constants of metal chelates attached to a protein. *J. Nucl. Med.* 1990; **31**(4): 480–488.